9964 *Biochemistry* **2010,** *49,* 9964–9971
DOI: 10.1021/bi1012996

BIOCHEMISTRY
including biophysical chemistry & molecular biology
*Article*

# Structure of the p53 Transactivation Domain in Complex with the Nuclear Receptor Coactivator Binding Domain of CREB Binding Protein[†]

Chul Won Lee, Maria A. Martinez-Yamout, H. Jane Dyson, and Peter E. Wright*

*Department of Molecular Biology and The Skaggs Institute for Chemical Biology, The Scripps Research Institute, 10550 North Torrey Pines Road, La Jolla, California 92037, United States*

*Received August 13, 2010; Revised Manuscript Received September 24, 2010*

ABSTRACT: The activity and stability of the tumor suppressor p53 are regulated by interactions with key cellular proteins such as MDM2 and CBP/p300. The transactivation domain (TAD) of p53 contains two subdomains (AD1 and AD2) and interacts directly with the N-terminal domain of MDM2 and with several domains of CBP/p300. Here we report the NMR structure of the full-length p53 TAD in complex with the nuclear coactivator binding domain (NCBD) of CBP. Both the p53 TAD and NCBD are intrinsically disordered and fold synergistically upon binding, as evidenced by the observed increase in helicity and increased level of dispersion of the amide proton resonances. The p53 TAD folds to form a pair of helices (denoted Pα1 and Pα2), which extend from Phe19 to Leu25 and from Pro47 to Trp53, respectively. In the complex, the NCBD forms a bundle of three helices (Cα1, residues 2066−2075; Cα2, residues 2081−2092; and Cα3, residues 2095−2105) with a hydrophobic groove into which p53 helices Pα1 and Pα2 dock. The polypeptide chain between the p53 helices remains flexible and makes no detectable intermolecular contacts with the NCBD. Complex formation is driven largely by hydrophobic contacts that form a stable intermolecular hydrophobic core. A salt bridge between D49 of p53 and R2105 of NCBD may contribute to the binding specificity. The structure provides the first insights into simultaneous binding of the AD1 and AD2 motifs to a target protein.

The p53 tumor suppressor acts as a hub in signal transduction networks that mediate the cellular response to stress, leading to cell cycle arrest, senescence, or apoptosis (*1*, *2*). Because of its role in determining cell fate, p53 is tightly controlled by numerous regulatory proteins, including MDM2,[1] MDMX, CBP/p300, and various kinases. In unstressed cells, p53 is maintained at extremely low levels through interactions with the ubiquitin E3 ligase MDM2 (*3*, *4*). This interaction results in ubiquitination and proteasomal degradation of p53 and also blocks interactions with the basal transcriptional proteins (*5*, *6*). MDMX, which is highly homologous to MDM2 but lacks ubiquitin ligase activity, also negatively regulates p53 and inhibits its transactivation function (*7*, *8*). Upon cellular stress, specific kinases that phosphorylate the N-terminal region of p53 are activated. Phosphorylation facilitates release from MDM2 and enhances binding to the general transcriptional coactivators CBP and p300 (*9*−*13*).

CBP and p300 function as scaffolds for the recruitment and assembly of the transcriptional machinery and modify both chromatin and transcription factors through their intrinsic acetyltransferase activity (*14*). They contain multiple protein interaction domains, including TAZ1, KIX, TAZ2, and a disordered C-terminal domain known variously as the nuclear receptor coactivator binding domain (NCBD) (*15*), the IRF-3 binding domain (IBiD) (*16*), and the SRC1 interaction domain (SID) (*17*) (shown schematically in Figure S1A of the Supporting Information). CBP and p300 play a central role in the p53 response and are required both for activation of p53-mediated transcription and for stabilization of the p53−DNA complex by acetylation of lysine residues in the C-terminal regulatory domain. Acetylation is necessary to inhibit the p53−MDM2 interaction and facilitate the p53-mediated stress response (*18*).

p53 is a modular protein that binds DNA as a tetramer; each subunit is comprised of an N-terminal transactivation domain (TAD, residues 1−61), a proline-rich domain (PRD), a core DNA binding domain, the tetramerization domain, and a C-terminal regulatory domain (Figure S1B of the Supporting Information). The p53 TAD interacts with CBP/p300 at multiple sites, and binding to one or more of the TAZ1, TAZ2, KIX, and NCBDs is required for CBP/p300-mediated transcription (*19*−*26*). The p53 TAD contains two subdomains, AD1 (residues 1−42) and AD2 (residues 43−63) (*27*−*30*), and is intrinsically disordered (*28*, *31*, *32*). NMR studies revealed that the free p53 TAD has a weak propensity to form transient helical structure between residues 18 and 26 and two turns (residues 40−44 and

[†]This work was supported by Grant CA96865 from the National Institutes of Health. C.W.L. was supported by a Korea Research Foundation Grant funded by the Korean Government (MOEHRD, Basic Research Promotion Fund) (KRF-2004-214-C00207).

*To whom correspondence should be addressed: Department of Molecular Biology and The Skaggs Institute for Chemical Biology, The Scripps Research Institute, 10550 N. Torrey Pines Rd., La Jolla, CA 92037. Phone: (858) 784-9721. Fax: (858) 784-9822. E-mail: wright@scripps.edu.

[1]Abbreviations: CD, circular dichroism; CBP, CREB binding protein; CREB, cyclic-AMP response element binding protein; DSS, sodium 2,2-dimethyl-2-silapentane-5-sulfonate; HDM2, human homologue of MDM2; MDM2, mouse double minute protein 2; HSQC, heteronuclear single-quantum coherence; IBiD, IRF-3 binding domain; IRF, interferon regulatory factor; ITC, isothermal titration calorimetry; MTSL, (1-oxyl-2,2,5,5-tetramethyl-$\Delta^3$-pyrrolin-3-yl)methyl methanethiosulfonate; NCBD, nuclear receptor coactivator binding domain; NMR, nuclear magnetic resonance; SID, SRC1 interaction domain; SRC1, steroid receptor coactivator 1; TAD, transactivation domain; TAZ, transcriptional adapter zinc finger.

 Published on Web 10/20/2010 

48−53) in solution (*33*, *34*). Regions within both AD1 and AD2 form stable helical structure upon binding to target proteins. Residues 18−26 in AD1 fold into an amphipathic helix upon binding to MDM2 (*35*), and helical structure is formed in AD2 upon binding to replication protein A and the Tfb1 subunit of TFIIH (*36*, *37*).

We showed previously that the AD1 and AD2 activation domains within the p53 TAD mediate interactions with CBP and HDM2 (*38*). Binding to CBP is dominated by interactions with AD2, while binding to HDM2 is mediated primarily by interactions involving AD1. The p53 TAD can bind simultaneously to HDM2 and to any one of the CBP domains, through the AD1 and AD2 motifs, respectively, to form a ternary complex (*39*).

In spite of the importance of the p53−CBP/p300 interaction, there is only limited structural information available for the complex between the AD1 region of the p53 TAD and the TAZ2 domain of p300 (*40*). To provide further insights into the structural basis for the recruitment of CBP/p300 by p53, we have determined the solution structures of the complex formed between the NCBD of CBP and residues 13−61 of the p53 TAD, encompassing both the AD1 and AD2 activation motifs. The NCBD is a key p53 binding site that contributes to activation of transcription of p53-responsive genes (*26*, *41*). The NCBD has been identified as the binding site for diverse proteins with little sequence similarity, including adenoviral E1A, interferon regulatory factor IRF-3, the p160 nuclear receptor coactivators ACTR, SRC1, and TIF-2, the human T-cell leukemia virus protein Tax, and p53, and undergoes large conformational changes upon binding to different protein targets (*16*, *42*, *43*). Upon binding to the NCBD, the AD1 and AD2 regions of the disordered p53 TAD fold to form helices that are stabilized by docking in a hydrophobic groove on the surface of the NCBD. The loop between AD1 and AD2 remains flexible and wraps around the third helix of the NCBD. Binding occurs primarily through hydrophobic interactions, and a salt bridge between D49 of p53 and R2105 of the NCBD may contribute to the specificity.

## EXPERIMENTAL PROCEDURES

*Protein Expression and Purification*. The NCBD (residues 2059−2117) domain of mouse CBP and constructs from the TAD of human p53 [p53(1−61), p53(13−61), and p53(38−61)] were expressed and purified as described previously (*38*, *42*). p53(25−61) was purified from protease digestion of p53(13−61) using trypsin (Sigma). Peptide p53(14−28) was synthesized on a Perseptive Biosystems synthesizer using solid-phase Fmoc methods as described previously (*38*). p53(13−61)D49A was engineered using site-directed mutagenesis and expressed and purified as described for the wild-type protein. For the NMR experiments, $^{15}$N-labeled or $^{13}$C- and $^{15}$N-labeled p53(13−61) and NCBDs were expressed in *Escherichia coli* BL21(DE3) [DNAY] in M9 minimal medium and purified. Spin-labeled [$^{15}$N]p53(13−61) was prepared by coupling MTSL to an N-terminal Cys residue, as described previously (*44*).

*Isothermal Titration Calorimetry* (*ITC*). Binding interactions were measured by isothermal titration calorimetry using a MicroCal Omega VP-ITC instrument (MicroCal, Amherst, MA), as previously described (*38*).

*NMR Sample Preparation*. For NMR experiments, p53(13−61) and NCBD were dissolved in 10 mM sodium phosphate (pH 6.5) and 50 mM NaCl. The solution of the complex was dialyzed in the same buffer. The dialyzed sample was exchanged into NMR buffer [10 mM sodium phosphate (pH 6.5) and 50 mM NaCl in a 10% $^2H_2O$/90% $H_2O$ mixture or 100% $^2H_2O$] using a Centriprep (Amicon). NMR samples contain a 1:1 p53:NCBD molar ratio, with the concentration of the proteins ranging from ~0.5 to 1 mM.

*NMR Spectroscopy*. All NMR experiments were performed on Bruker 600, 750, 800, and 900 MHz spectrometers at 298 K. NMR spectra were referenced to external DSS. NMR data processing and analysis were performed using NMRPipe (*45*) and NMRView (*46*). Backbone resonance assignment was accomplished using standard HNCA (*47*), HNCACB (*48*), and CBCA(CO)NH (*47*) triple-resonance experiments. Assignments of side chain resonances were made using three-dimensional (3D) HCCH-COSY and HCCH-TOCSY experiments (*49*). Torsion angle restraints were derived from 3D HACAHB-COSY (*50*), HNHB (*51*), and HNHA (*52*) data sets. Distance restraints were derived from 3D $^{15}$N-edited NOESY-HSQC ($\tau_m$ = 100 and 150 ms) and $^{13}$C-edited NOESY-HSQC ($\tau_m$ = 100 and 150 ms) spectra. Intermolecular NOEs used in structure calculations were obtained from $^{13}$C-filtered, $^{12}$C-edited NOESY-HSQC and $^{13}$C-edited, $^{12}$C-filtered NOESY-HSQC ($\tau_m$ = 200 ms) experiments.

*Structure Calculations and Analyses*. A total of 65 unambiguous intermolecular NOEs were manually assigned and used for the structure calculations. Initial structure calculations were conducted with CYANA (*53*) with CANDID (*54*). Hydrogen bonds for the helical regions of the NCBD were added to facilitate the automated assignment of additional NOE restraints by CANDID but were removed during the structure refinement. Chemical shift-based restraints from TALOS (*55*) were included only for helical regions. On the basis of the coupling constants and NOE patterns, 14 side chain $\chi_1$ angles were restrained to −60° ± 30°, 60° ± 30°, and 180° ± 30°.

The initial set of 100 structures generated in CYANA version 2.1 with the redundant dihedral angle constraints (REDAC) (*56*) was further refined by molecular dynamics calculations with AMBER9 under in vacuo conditions with 20% reduced charges (*57*). Iterative refinement and editing of the distance restraints based on the NOESY spectra to remove incorrect and ambiguous assignments reduced the number of restraints. Final refinement in AMBER9 incorporated the generalized Born solvent model (*58*). Force constants were 20 kcal mol$^{-1}$ Å$^{-2}$ for NOE restraints and 200 kcal mol$^{-1}$ rad$^{-2}$ for dihedral angle restraints. The 20 structures with the lowest generalized Born AMBER energy were chosen for analysis using PROCHECK-NMR (*59*). Figures were prepared using MOLMOL (*60*).

*Spin Labeling Experiment*. A spin-labeled NMR sample was prepared in NMR buffer at a molar ratio of 1:1 for N-terminally spin-labeled [$^{15}$N]p53(13−61) and unlabeled NCBD. For measurements of paramagnetic relaxation enhancement, $^1$H−$^{15}$N HSQC spectra were recorded in the presence and absence of ascorbic acid. Reduction of the spin-label to its diamagnetic state was achieved by addition of a 5-fold molar excess of ascorbic acid and incubation overnight. The intensity ratios of $^1$H−$^{15}$N HSQC peaks were calculated as $I_{para}/I_{dia}$, where $I_{para}$ is the resonance intensity of the spin-labeled sample and $I_{dia}$ is the resonance intensity of the spin-labeled sample following reduction with ascorbic acid

## RESULTS

To dissect the interactions between p53 TAD and NCBD, we prepared p53 constructs encompassing the full-length TAD

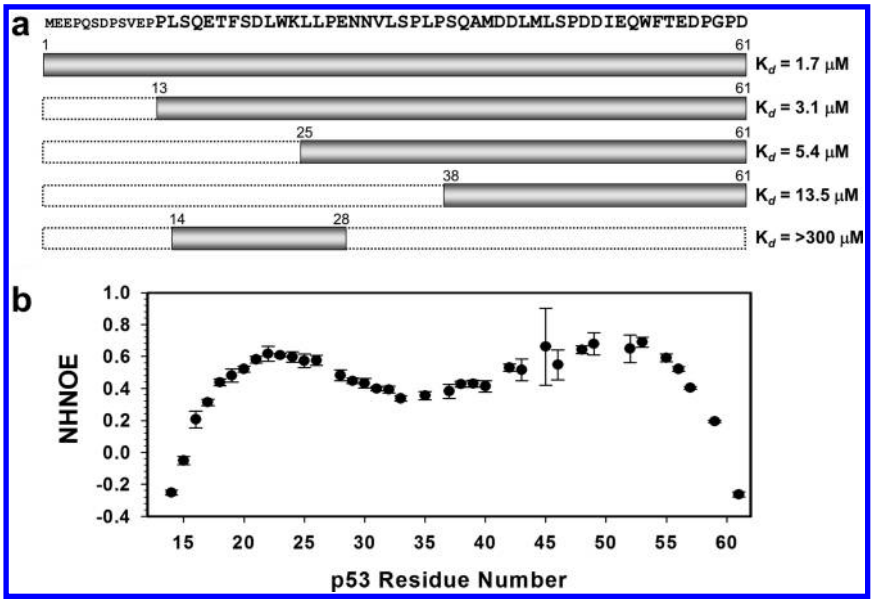


FIGURE 1: Binding affinity of p53 TADs for NCBD and p53 TAD binding region. (a) Schematic drawing of various p53 TADs. The dissociation constants ($K_d$) of each domain are indicated. (b) Heteronuclear $^1H-^{15}N$ NOE for [$^{15}N$]p53(13−61) bound to NCBD.

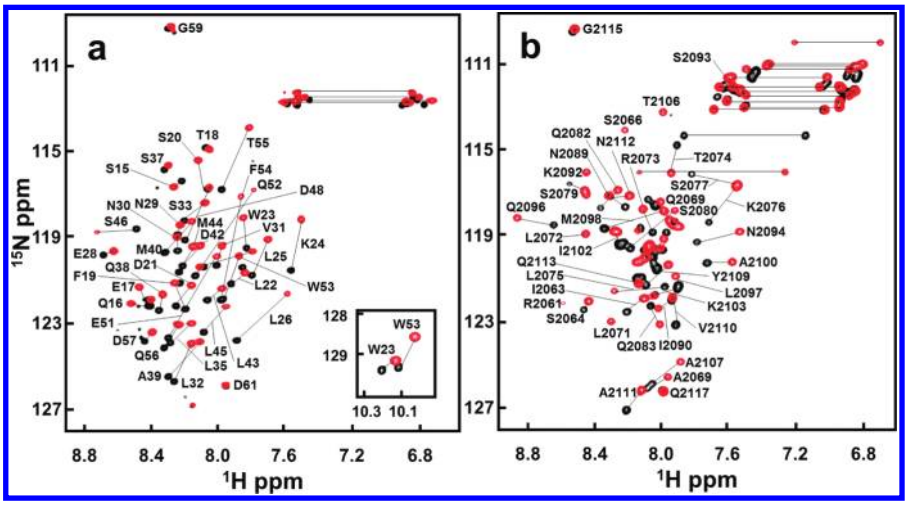


FIGURE 2: $^1H-^{15}N$ HSQC spectra of the p53 TAD and NCBD. (a) [$^{15}N$]p53(13−61) free (black) and in the presence (1:1) of unlabeled NCBD (red). Peaks from two tryptophan side chains are shown in the inset. (b) [$^{15}N$]NCBD free (black) and in the presence (1:1) of unlabeled p53(13−61) (red).

(residues 1−61) and various truncated peptides (residues 13−61, 25−61, 14−28, and 38−61; the latter two peptides encompass the isolated AD1 and AD2 subdomains, respectively). The interactions between the p53 TAD constructs and the NCBD were investigated by both ITC and NMR, and the measured dissociation constants ($K_d$) are summarized in Figure 1a. The longest peptide, p53(1−61), binds with the highest affinity, while the N-terminally truncated peptides p53(13−61) and p53(25−61) bind ~2−3-fold more weakly. The peptides representing the isolated AD1 and AD2 subdomains bind approximately 170- and 8-fold more weakly than p53(1−61), respectively. These results indicate that binding of the p53 TAD to the NCBD is dominated by the AD2 region, although the AD1 region does contribute somewhat to the overall binding affinity.

*Mutual Synergistic Folding between the p53 TAD and CBP NCBD*. The p53 TAD in the unbound state is intrinsically disordered, as evidenced by the limited dispersion in the $^1H-^{15}N$ HSQC spectrum (Figure 2) and by a circular dichroism spectrum that is characteristic of a random coil (Figure S2 of the Supporting Information). The free NCBD is not entirely unstructured but forms a helical state with the characteristics of a molten globule (*42*). Formation of a complex is accompanied by a significant increase in the level of dispersion of the $^1H-^{15}N$ HSQC spectra (Figure 2) and the increased helicity of the CD spectra of the bound state (Figure S2 of the Supporting Information), showing that both proteins fold upon binding. Binding to the NCBD also results in shifts of the $^{13}C\alpha$ resonances in two regions of p53, confirming formation of helical structure between residues 19−24 and 47−53 in the complex (Figure S3a of the Supporting Information). Slight increases in the level of helical structure are also observed for the NCBD in the bound state (Figure S3b of the Supporting Information).

*Structure Determination*. The structure of the complex formed between the NCBD and p53(13−61) was determined using constraints derived from heteronuclear multidimensional NMR experiments. We opted to use the N-terminally truncated p53 TAD (residues 13−61) rather than the full-length TAD for structure determination because the affinities of p53(1−61) and p53(13−61) for NCBD are similar (differing by less than 2-fold); residues N-terminal to Thr18 display anomalously small $^1H-^{15}N$

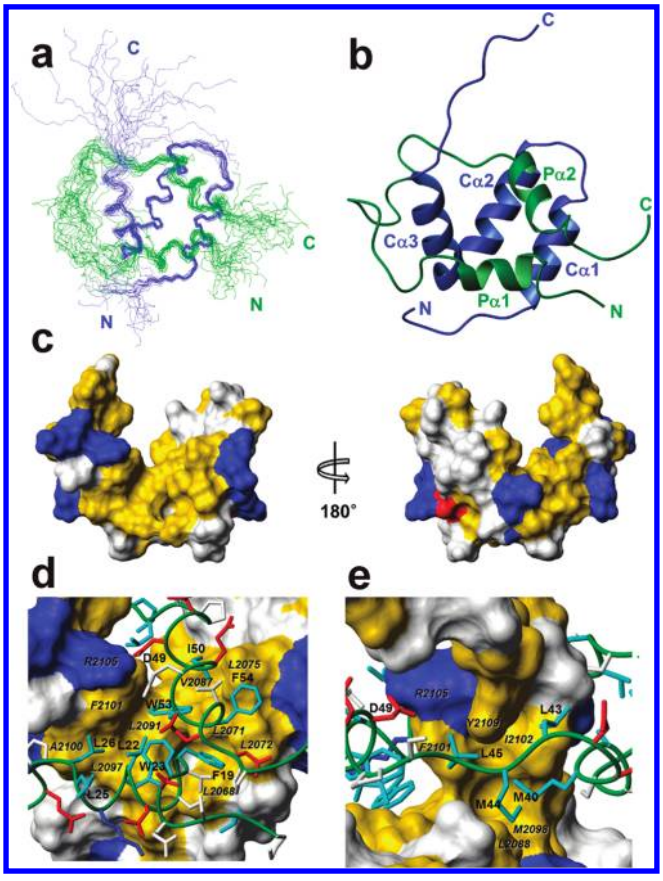


FIGURE 3: Solution structure of the p53 TAD−NCBD complex. (a) Best 20 structures superposed on backbone heavy atoms in ordered regions. The p53 TAD backbone is colored green and the NCBD blue, and the N- and C-termini of each chain are labeled in the corresponding colors. (b) Ribbon representation, in the same orientation and color as panel a. Helices Pα1−2 and Cα1−3 and N- and C-termini are labeled. (c) Surface representation of the NCBD in complex with the p53 TAD. The left and right panels are rotated 180° relative to one another about a vertical axis. Hydrophobic residues (Ala, Met, Leu, Ile, Val, Phe, and Tyr) are colored yellow; positively charged (Arg and Lys) and negatively charged (Asp) residues are colored blue and red, respectively. The other residues are colored white. (d and e) Binding site for Pα1 and Pα2 and extended region of the p53 TAD (green tube) in the hydrophobic grooves on the surface of the NCBD. The surfaces of interacting hydrophobic side chains from NCBD are labeled in black italic characters. The side chains of basic and acidic residues of p53 TAD are colored blue and red, respectively. The side chains of hydrophobic residues of the p53 TAD are colored cyan and labeled. The side chains of other residues are colored white.

heteronuclear NOEs in the complex (Figure 1b) and appear not to interact with the NCBD. To minimize spectral overlap and simplify the assignment process, complexes were formed with only one component labeled with $^{15}$N or with $^{13}$C and $^{15}$N and the other unlabeled. In contrast to the free proteins, the NMR spectra of the p53 TAD and NCBD in the complex are well dispersed and allow for nearly complete resonance assignment (~95% of the $^{1}$H, $^{13}$C, and $^{15}$N resonances).

Initially, 24 spectroscopically unambiguous intermolecular NOEs between the p53 TAD and the NCBD were assigned manually and used as restraints in the first round of CYANA structure calculations. An additional 41 intermolecular NOE restraints were assigned using CANDID. These CANDID-assigned intermolecular NOEs were subsequently checked and verified against the filtered NOESY spectra ($^{13}$C-filtered, $^{12}$C-edited NOESY-HSQC, and $^{13}$C-edited, $^{12}$C-filtered NOESY-HSQC) of both [$^{13}$C,$^{15}$N]p53 TAD−unlabeled NCBD and [$^{13}$C,$^{15}$N]NCBD−unlabeled p53 TAD complexes. A total of 1503 distance restraints and 132 torsion angle restraints were used in the final rounds of structure calculation and refinement. The 20 structures with the lowest AMBER energies are shown in Figure 3a, and the structural statistics are summarized in Table 1. All residues in structured regions have low root-mean-square deviation (rmsd) values (0.61 Å for backbone atoms and 0.93 Å for all heavy atoms). There are no dihedral angle violations in the final ensemble of 20 structures; the maximal NOE distance violation is 0.25, and all residues are in allowed regions of the Ramachandran plot.

Table 1: NMR Restraints and Structural Statistics

| NMR Constraints | NCBD | p53 TAD |
|---|---|---|
| total no. of NOE distance restraints | 836 | 602 |
| intraresidue ($i$, $i$) | 245 | 178 |
| sequential ($i$, $i+1$) | 260 | 258 |
| medium-range ($2 \le \lvert i-j \rvert \le 4$) | 247 | 154 |
| long-range ($\lvert i-j \rvert \ge 5$) | 84 | 12 |
| intermolecular | 65 | |
| no. of dihedral angle restraints | | |
| $\phi$ | 47 | 26 |
| $\psi$ | 33 | 12 |
| $\chi_1$ | 7 | 7 |

| Structural Statistics (20 structures) | |
|---|---|
| no. of AMBER restraint violations | |
| maximal NOE violation (Å) | 0.25 |
| maximal torsion angle violation (deg) | 0 |
| deviations from ideal geometry | |
| bond lengths (Å) | 0.0102 ± 0.0001 |
| bond angles (deg) | 2.10 ± 0.02 |
| AMBER energies (kcal/mol) | |
| mean restraint energy | 9.2 |
| mean AMBER energy | −3745.9 |
| rmsd from the mean[a] | |
| backbone heavy atoms (Å) | 0.61 |
| heavy atoms (Å) | 0.93 |
| PROCHECK statistics | |
| most favored region (%) | 84.8 |
| additionally allowed region (%) | 14.8 |
| generously allowed region (%) | 0.4 |
| disallowed region (%) | 0.0 |

[a]Analysis included residues P2065−R2105 (NCBD) and F19−W23 and P47−F54 (p53 TAD).

*Overall Structure of the p53 TAD−NCBD Complex*. In the bound state, the p53 TAD comprises two helical regions (denoted Pα1 and Pα2) that extend from Phe19 to Leu25 and from Pro47 to Trp53, respectively (Figure 3b). The N- and C-terminal residues and residues around positions 27−39, which form a long loop between helices Pα1 and Pα2, are disordered in the structure ensemble (Figure 3a) in accord with their small heteronuclear NOEs (Figure 1b), sharp resonances, and the lack of intermolecular NOEs for these residues.

The NCBD is composed of three α-helices (Cα1, residues 2066−2075; Cα2, residues 2081−2092; and Cα3, residues 2095−2105) that pack to expose a broad hydrophobic groove into which helices Pα1 and Pα2 of p53 dock (Figure 3b,c).

The helices of p53 are close to each other in the complex, as evidenced by long-range intramolecular NOEs between these regions and spin labeling experiments; a paramagnetic spin-label attached through a cysteine residue at the N-terminus of

Table 2: Thermodynamic Parameters Obtained from Isothermal Titration Calorimetry Experiments for Complexes of p53 TADs and the NCBD

| complex | $\Delta H$ (kcal/mol) | $-T\Delta S$ (kcal/mol) | $K_d$ ($\mu$M) |
|---|---|---|---|
| p53(13−61)−NCBD | −4.42 ± 0.15 | −3.37 ± 0.19 | 3.1 ± 0.2 |
| p53(13−61)D49A−NCBD | −2.09 ± 0.45 | −5.37 ± 0.41 | 5.1 ± 0.3 |
| p53(25−61)−NCBD | −4.12 ± 0.46 | −3.32 ± 0.59 | 5.4 ± 1.8 |
| p53(38−61)−NCBD | −4.60 ± 0.12 | −2.26 ± 0.10 | 13.5 ± 0.54 |

p53(13−61) causes broadening of resonances from residues in both Pα1 and Pα2 (Figure S4 of the Supporting Information). The loop of residues 27−39 of p53 wraps around helix Cα3 of the NCBD but appears to form no persistent contacts because it does not give rise to any detectable intermolecular NOEs.

*p53 TAD−NCBD Interface*. The interface between the NCBD and helices Pα1 and Pα2 of the p53 TAD is predominantly hydrophobic (Figure 3c). Several basic residues are located around this hydrophobic surface and form complementary electrostatic interactions with acidic side chains of the p53 TAD. Helix Pα1 of p53 occupies a region of the hydrophobic groove formed by L2068, L2072, L2097, and F2101 in helices Cα1 and Cα3 of the NCBD. In addition, L26 of p53 makes a hydrophobic contact with A2100 and F2101 of the NCBD (Figure 3d). Four hydrophobic residues (M40, L43, M44, and L45) of p53 bind to the top of the hydrophobic groove formed by Cα2 and Cα3, packing against L2088, M2098, F2101, and I2102 of the NCBD (Figure 3e). The second helix of p53 (Pα2) interacts with the side chains of L2071, L2072, L2075, V2087, L2091, and F2101 of the NCBD. The two Trp and two Phe residues in Pα1 and Pα2 are deeply buried within the hydrophobic interface between p53 and the NCBD. Long-range NOEs between Pα1 and Pα2, including F19−W53, L22−Q52, and L22−W53 NOEs, were detected in the NOESY-HSQC spectra, providing direct spectroscopic confirmation of the proximal location of these helices.

The total buried hydrophobic surface area is 880 Å$^2$, of which 580 Å$^2$ is contributed by helix Pα2 and the neighboring residues 40−45; the remainder of the hydrophobic surface is buried by helix Pα1 of p53. There is a salt bridge between D49 of the p53 TAD and R2105 of the NCBD that may contribute to binding specificity (Figure 3e). Substitution of D49 with Ala decreases the binding affinity only slightly but significantly changes the energetics of the interaction between the p53 TAD and NCBD (Table 2). Other short truncated p53 TADs containing D49 showed similar favorable enthalpy changes ($\Delta H$) with p53(13−61) (Table 2), indicating that the salt bridge between D49 of the p53 TAD and R2106 of the NCBD does play a role in the formation of the complex.

## DISCUSSION

*Structure of the p53 TAD*. The N-terminal region of p53 consists of two domains, the transcriptional activation domain (TAD) and a proline-rich domain (PRD), that are directly involved in protein−protein interactions, post-translational modifications, and regulation of activity of p53. The PRD has a tendency to adopt polyproline II structure in full-length p53, as shown by NMR and SAXS (*61*). The unbound TAD is intrinsically disordered, although transient local structures and long-range interactions have been observed in NMR experiments (*34*, *62*). The TAD contains two subdomains, AD1 and AD2, that mediate the interactions of p53 with MDM2 and CBP/p300 (*35*, *38*, *63*). The AD1 region is the primary binding site for MDM2 and folds into an amphipathic α-helix (residues 18−26) upon complex formation (Figure 4a). The p53 TAD interacts with replication protein A (RPA) and the Tfb1/p62 subunit of TFIIH by way of the AD2 subdomain. Binding to RPA causes AD2 to fold to form two short helices, located between residues 41 and 44 and between residues 47 and 55 (Figure 4a). Residues 47−55 also fold into a helical structure when AD2 binds to the Tfb1 subunit of TFIIH (Figure 4a). Binding to CBP/p300 is also dominated by interactions with AD2; the p53 TAD can bind simultaneously to MDM2 and to TAZ1, TAZ2, KIX, or NCBDs of CBP/p300 through the AD1 and AD2 motifs, respectively, to form a ternary complex (*38*).

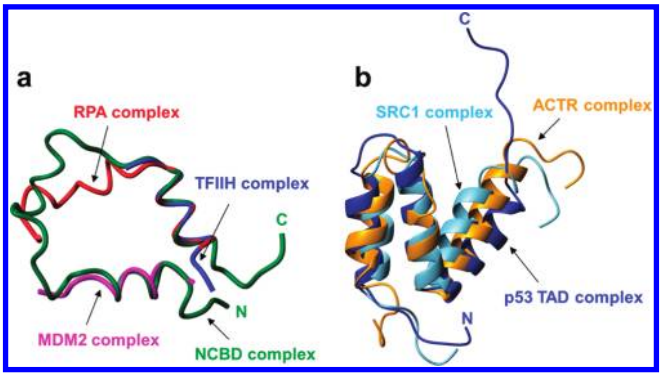


FIGURE 4: Superposition of p53 TAD and NCBD structures. (a) The backbone of the p53 TAD in the complex with NCBD is shown as a green tube. The p53 TAD structures in the complex with other proteins are aligned on the backbone heavy atoms of Pα1 and Pα2 of the p53 TAD in the complex with NCBD. The AD1 region of the p53 TAD in the complex with MDM2 is colored magenta. The AD2 region of the p53 TAD in the complexes with RPA and TFIIH is colored red and blue, respectively. (b) Superposition of the structures adopted by the NCBD in complexes with the p53 TAD (blue), ACTR (orange), and SRC1 (cyan). The NCBD backbone is shown as a ribbon, and the structures are superimposed on the backbone heavy atoms of residues in helices Cα1 and Cα2 of the NCBD.

To date, all structures reported for the p53 TAD have been for the isolated AD1 or AD2 subdomains only. In this work, we determined structures of the full-length TAD, encompassing both the AD1 and AD2 regions, in complex with the NCBD of CBP. Both AD1 and AD2 interact directly with the NCBD, and each subdomain folds upon binding to form a helical motif (Pα1, residues 19−25, and Pα2, residues 47−53). Residues 40−45 of p53, which adopt helical structure in the RPA complex, also contribute to the binding to the NCBD, although apparently without formation of regular secondary structure. The helical regions of the p53 TAD are very similar in the complexes with the NCBD, MDM2, RPA, and Tfb1 (Figure 4a), suggesting that formation of a conserved local structure is a feature of p53 recognition.

*Structure of the NCBD*. The free CBP NCBD exhibits the spectroscopic and thermodynamic characteristics of a molten globule; although helices Cα1 and Cα2 are almost fully folded and helix Cα3 is partly formed in the free NCBD, the protein is not cooperatively folded and displays inherent flexibility (*15*, *42*, *64*). The level of folding of the NCBD is induced upon interaction with its binding partners (*16*, *42*). Although the NCBD is stabilized as a three-helix bundle in all of its complexes, the length of the helices and the packing topology differ significantly in complexes with different binding partners. In particular, the NCBD adopts a very different conformation in its complex with the globular protein IRF-3 (*65*) than it does when bound to the disordered interaction domains of the nuclear receptor coactivators ACTR and

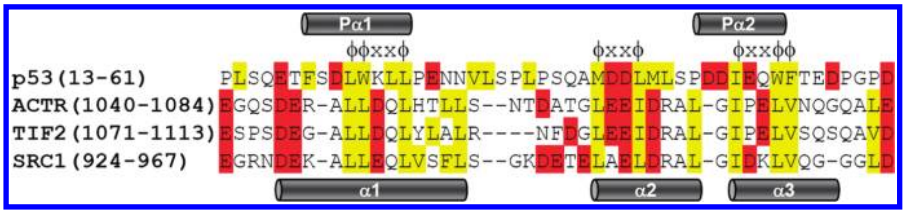


FIGURE 5: Alignment of the amino acid sequences of NCBD binding proteins. Conserved amino acids are colored according to type: hydrophobic residues (Ala, Val, Ile, Leu, Met, Phe, and Tyr) colored a shade of yellow and negatively charged residues (Asp and Glu) colored red. The conserved motifs ($\phi\phi$XX$\phi$,$\phi$XX$\phi$, or $\phi$XX$\phi\phi$, where $\phi$ represents a hydrophobic amino acid and X represents any amino acid) are shown over the sequence alignment. α-Helical regions of the p53 TAD and ACTR in the complex with the NCBD are shown over the alignment and under the alignment, respectively.

SRC1 (*42*, *65*, *66*). Figure 4b shows a superposition of the NCBD structure in its complexes with the p53 TAD, ACTR, and SRC1. While the overall fold of the NCBD is similar in these three complexes (the backbone rmsd in the structured regions is 1.4 Å), some differences are observed in the length and orientation of helix Cα3. This helix is extended by an extra turn in the C-terminus in the ACTR complex, presumably as a consequence of extensive hydrophobic contacts with the third helix of ACTR (*42*). The angle between helices Cα2 and Cα3 of the NCBD is larger (67°) in the p53 TAD complex than in the complex with ACTR (58°). This may reflect the fact that the two helices (Pα1 and Pα2) of the p53 TAD are packed across the hydrophobic groove of the NCBD, compared to a single helix lying along the groove in the ACTR and SRC1 complexes. In addition, the binding affinities are very different for the NCBD complexes with ACTR and the p53 TAD ($K_d$ = 0.034 vs 3.1 $\mu$M). The Cα2 helix is observed to be slightly shorter in the ACTR complex than in the p53 or SRC1 structures; however, this difference probably reflects the lack of resonance assignments and a corresponding lack of restraints for the poly-Q segment (residues 2082−2086) of the ACTR complex, rather than real structural differences.

*Recognition of the NCBD by the p53 TAD*. A helical region containing the LXXLL motif mediates the interactions among CBP/p300, p160 coactivators, and the ligand-binding domains of nuclear receptors (*67*−*70*). Similar motifs, with $\phi\phi$XX$\phi$ or $\phi$XX$\phi\phi$ sequence patterns, where $\phi$ is a bulky hydrophobic residue (commonly leucine) and X is any other residue, directly mediate the interaction between the NCBD and ACTR (Figure 5) (*42*). These motifs are also found in the AD1 and AD2 regions of the p53 TAD (Figure 5), although the mode of interaction with the NCBD is different from that of ACTR. The hydrophobic residues in AD2 (M40, L43, M44, L45, I50, W53, and F54) are directly involved in interactions with the NCBD, in the deep groove formed between helices Cα1 and Cα2 and helix Cα3. Residues 40−45 appear to be less well ordered and have a smaller heteronuclear NOE than residues in helices Pα1 and Pα2, but this region of the p53 backbone exhibits a tendency toward a distorted helical conformation in the ensemble of p53−NCBD complex structures. In addition, F19, W23, and L26 in the AD1 region also interact with the hydrophobic surface formed between helices Cα1 and Cα3. The L22Q or W23S point mutation does not significantly impair binding of p53 to the NCBD (*26*), indicating that the hydrophobic residues in AD2 are essential for stabilizing the hydrophobic core of the complex. L2068 and L2071 of the NCBD make a hydrophobic contact with F19 and F54, respectively, of the p53 TAD. The double mutation in which both NCBD residues are replaced with alanine (L2068A/L2071A) has a significant effect on p53 binding (*26*), indicating that F19 and F54 are also critical for complex formation. Mutation of hydrophobic residues in AD2 impairs binding of p53 to the NCBD; the double mutant W53Q/F54S binds with ~3-fold lower affinity than the wild-type TAD (*63*). Simultaneous mutation of both AD1 and AD2 (L22Q/W23S and W53Q/F54S) has much more deleterious effects on binding (*63*), indicating that the hydrophobic residues in AD1 and AD2 are synergistically involved in the binding to the NCBD. These data are fully consistent with our structure of the p53 TAD−NCBD complex, in which both AD1 and AD2 simultaneously interact with the NCBD.

Although the interface between the p53 TAD and the NCBD is predominantly hydrophobic, a salt bridge (between D49 of p53 and R2105 of the NCBD) also contributes to the interaction. In the ACTR−NCBD complex, R2105 of NCBD makes a salt bridge with D1068 of ACTR to provide binding specificity but does not contribute significantly to binding affinity or stability (*15*, *42*). The single substitution of the salt bridge (NCBD R2105L) has a relatively minor effect on the $K_d$ of the complex but causes a reduction in the favorable enthalpy change upon binding. In the complex between the p53 TAD and NCBD, we observe similar energetic effects from disruption of the salt bridge via substitution of D49 of p53 with alanine; the mutation has an only minor effect on the $K_d$ but causes a 2-fold reduction in the favorable enthalpy change that accompanies binding ($\Delta H$ of −2.1 kcal/mol for D49A vs −4.4 kcal/mol for wild-type p53). Therefore, as with ACTR, the salt bridge in the p53 TAD−NCBD complex may contribute to specificity rather than binding affinity. Thus, it appears that R2105 of the NCBD may play a general role in target selection among the many nuclear proteins that use amphipathic helical motifs for recognition.

*Structural and Functional Malleability of p53*. Human p53 contains large disordered regions, including N-terminal and C-terminal domains that interact with more than one protein. Short recognition domains embedded in disordered regions in eukaryotic transcriptional complexes can lead to structural and functional malleability that provides adaptability for the recognition of multiple targets having different structures (*71*). The N-terminal transactivation domain of p53 interacts with several partners, including CBP/p300, RPA, Tfb1, and MDM2. Although the two short binding domains (AD1 and AD2) in the p53 TAD are structurally homologous motifs that form an amphipathic helix upon binding to their target proteins, their functions are distinct. Binding of the p53 TAD to CBP/p300, RPA, and Tfb1 is dominated by interaction with AD2. In contrast, binding of the p53 TAD to MDM2 is mediated primarily by AD1; however, upon phosphorylation of p53 at Thr18 in response to DNA damage, MDM2 is released and the p53 TAD binds preferentially to the NCBD and other domains of CBP/p300 (*38*). Our present structure shows that, in the absence of MDM2, both the AD1 and AD2 motifs of the p53 TAD interact with the NCBD, and that the 13 residues between them remain disordered in the bound form. While binding is dominated by the AD2 motif [$K_d$ = 5−14 $\mu$M for

peptides containing only AD2, and $K_d > 300\ \mu M$ for the isolated AD1 peptide (Figure 1)], both AD1 and AD2 contribute to the overall affinity for binding to the NCBD. AD1 and AD2 essentially function as clamps, connected by a disordered linker that does not make direct contacts with the NCBD. A clamp model of binding has been observed for other intrinsically disordered proteins, leading to an enhancement of binding affinity compared to that of the isolated motifs and providing flexibility and adaptability in molecular interactions (*72*). In the case of p53, the presence of two interaction motifs in the intrinsically disordered TAD imparts the flexibility to form ternary complexes with MDM2 and CBP/p300 domains or to bind with enhanced affinity through clamplike interactions with the NCBD or other CBP/p300 domains (*38*).

## ACKNOWLEDGMENT

We thank Josephine Ferreon for providing ITC data on the interaction of the NCBD with p53(1−61), Mindy Landes and Euvel Manlapaz for help with sample preparation, and John Chung and Gerard Kroon for expert assistance with NMR data collection.

## SUPPORTING INFORMATION AVAILABLE

Schematic diagram showing the domains of CBP and p53 with their abbreviations (Figure S1), CD spectra of the free proteins and the complexes (Figure S2), graphs of Cα secondary chemical shifts for each component of the complex (Figure S3), and a graph showing the locations of paramagnetic relaxation enhancement to spin relaxation for p53(13−61) (Figure S4). This material is available free of charge via the Internet at http://pubs.acs.org.

## REFERENCES

1. Greenblatt, M. S., Bennett, W. P., Hollstein, M., and Harris, C. C. (1994) Mutations in the p53 tumor suppressor gene: Clues to cancer etiology and molecular pathogenesis. *Cancer Res. 54*, 4855–4878.
2. Soussi, T., and Beroud, C. (2001) Assessing TP53 status in human tumours to evaluate clinical outcome. *Nat. Rev. Cancer 1*, 233–240.
3. Moll, U. M., and Petrenko, O. (2003) The MDM2-p53 interaction. *Mol. Cancer Res. 1*, 1001–1008.
4. Brooks, C. L., and Gu, W. (2006) p53 ubiquitination: Mdm2 and beyond. *Mol. Cell 21*, 307–315.
5. Momand, J., Zambetti, G. P., Olson, D. C., George, D., and Levine, A. J. (1992) The mdm-2 oncogene product forms a complex with the p53 protein and inhibits p53-mediated transactivation. *Cell 69*, 1237–1245.
6. Thut, C. J., Goodrich, J. A., and Tjian, R. (1997) Repression of p53-mediated transcription by MDM2: A dual mechanism. *Genes Dev. 11*, 1974–1986.
7. Toledo, F., and Wahl, G. M. (2006) Regulating the p53 pathway: In vitro hypotheses, in vivo veritas. *Nat. Rev. Cancer 6*, 909–923.
8. Toledo, F., Krummel, K. A., Lee, C. J., Liu, C. W., Rodewald, L. W., Tang, M., and Wahl, G. M. (2006) A mouse p53 mutant lacking the proline-rich domain rescues Mdm4 deficiency and provides insight into the Mdm2-Mdm4-p53 regulatory network. *Cancer Cell 9*, 273–285.
9. Lambert, P. F., Kashanchi, F., Radonovich, M. F., Shiekhattar, R., and Brady, J. N. (1998) Phosphorylation of p53 serine 15 increases interaction with CBP. *J. Biol. Chem. 273*, 33048–33053.
10. Dumaz, N., and Meek, D. W. (1999) Serine15 phosphorylation stimulates p53 transactivation but does not directly influence interaction with HDM2. *EMBO J. 18*, 7002–7010.
11. Sakaguchi, K., Saito, S., Higashimoto, Y., Roy, S., Anderson, C. W., and Appella, E. (2000) Damage-mediated phosphorylation of human p53 threonine 18 through a cascade mediated by a casein 1-like kinase. Effect on Mdm2 binding. *J. Biol. Chem. 275*, 9278–9283.
12. Dornan, D., and Hupp, T. R. (2001) Inhibition of p53-dependent transcription by BOX-I phospho-peptide mimetics that bind to p300. *EMBO Rep. 2*, 139–144.
13. Schon, O., Friedler, A., Bycroft, M., Freund, S. M., and Fersht, A. R. (2002) Molecular mechanism of the interaction between MDM2 and p53. *J. Mol. Biol. 323*, 491–501.
14. Goodman, R. H., and Smolik, S. (2000) CBP/p300 in cell growth, transformation, and development. *Genes Dev. 14*, 1553–1577.
15. Demarest, S. J., Deechongkit, S., Dyson, H. J., Evans, R. M., and Wright, P. E. (2004) Packing, specificity, and mutability at the binding interface between the p160 coactivator and CREB-binding protein. *Protein Sci. 13*, 203–210.
16. Lin, C. H., Hare, B. J., Wagner, G., Harrison, S. C., Maniatis, T., and Fraenkel, E. (2001) A small domain of CBP/p300 binds diverse proteins: Solution structure and functional studies. *Mol. Cell 8*, 581–590.
17. Sheppard, H. M., Harries, J. C., Hussain, S., Bevan, C., and Heery, D. M. (2001) Analysis of the steroid receptor coactivator 1 (SRC1)-CREB binding protein interaction interface and its importance for the function of SRC1. *Mol. Cell. Biol. 21*, 39–50.
18. Tang, Y., Zhao, W., Chen, Y., Zhao, Y., and Gu, W. (2008) Acetylation is indispensable for p53 activation. *Cell 133*, 612–626.
19. Avantaggiati, M. L., Ogryzko, V., Gardner, K., Giordano, A., Levine, A., and Kelly, K. (1997) Recruitment of p300/CBP in p53-dependent signal pathways. *Cell 89*, 1175–1184.
20. Gu, W., Shi, X. L., and Roeder, R. G. (1997) Synergistic activation of transcription by CBP and p53. *Nature 387*, 819–823.
21. Lill, N. L., Grossman, S. R., Ginsberg, D., DeCaprio, J., and Livingston, D. M. (1997) Binding and modulation of p53 by p300/CBP coactivators. *Nature 387*, 823–827.
22. Scolnick, D. M., Chehab, N. H., Stavridi, E. S., Lien, M. C., Caruso, L., Moran, E., Berger, S. L., and Halazonetis, T. D. (1997) CREB-binding protein and p300/CBP-associated factor are transcriptional coactivators of the p53 tumor suppressor protein. *Cancer Res. 57*, 3693–3696.
23. Grossman, S. R., Perez, M., Kung, A. L., Joseph, M., Mansur, C., Xiao, Z. X., Kumar, S., Howley, P. M., and Livingston, D. M. (1998) p300/MDM2 complexes participate in MDM2-mediated p53 degradation. *Mol. Cell 2*, 405–415.
24. Van Orden, K., Giebler, H. A., Lemasson, I., Gonzales, M., and Nyborg, J. K. (1999) Binding of p53 to the KIX domain of CREB binding protein: A potential link to human T-cell leukemia virus, type I-associated leukemogenesis. *J. Biol. Chem. 274*, 26321–26328.
25. Wadgaonkar, R., and Collins, T. (1999) Murine double minute (MDM2) blocks p53-coactivator interaction, a new mechanism for inhibition of p53-dependent gene expression. *J. Biol. Chem. 274*, 13760–13767.
26. Livengood, J. A., Scoggin, K. E. S., van Orden, K., McBryant, S. J., Edayathumangalam, R. S., Laybourn, P. J., and Nyborg, J. K. (2002) p53 transcriptional activity is mediated through the SRC1-interacting domain of CBP/p300. *J. Biol. Chem. 277*, 9054–9061.
27. Unger, T., Mietz, J. A., Scheffner, M., Yee, C. L., and Howley, P. M. (1993) Functional domains of wild-type and mutant p53 proteins involved in transcriptional regulation, transdominant inhibition, and transformation suppression. *Mol. Cell. Biol. 13*, 5186–5194.
28. Chang, J., Kim, D. H., Lee, S. W., Choi, K. Y., and Sung, Y. C. (1995) Transactivation ability of p53 transcriptional activation domain is directly related to the binding affinity to TATA-binding protein. *J. Biol. Chem. 270*, 25014–25019.
29. Candau, R., Scolnick, D. M., Darpino, P., Ying, C. Y., Halazonetis, T. D., and Berger, S. L. (1997) Two tandem and independent sub-activation domains in the amino terminus of p53 require the adaptor complex for activity. *Oncogene 15*, 807–816.
30. Zhu, J., Zhou, W., Jiang, J., and Chen, X. (1998) Identification of a novel p53 functional domain that is necessary for mediating apoptosis. *J. Biol. Chem. 273*, 13030–13036.
31. Ayed, A., Mulder, F. A., Yi, G. S., Lu, Y., Kay, L. E., and Arrowsmith, C. H. (2001) Latent and active p53 are identical in conformation. *Nat. Struct. Biol. 8*, 756–760.
32. Dawson, R., Muller, L., Dehner, A., Klein, C., Kessler, H., and Buchner, J. (2003) The N-terminal domain of p53 is natively unfolded. *J. Mol. Biol. 332*, 1131–1141.
33. Botuyan, M. V. E., Momand, J., and Chen, Y. (1997) Solution conformation of an essential region of the p53 transactivation domain. *Folding Des. 2*, 331–342.
34. Lee, H., Mok, K. H., Muhandiram, R., Park, K. H., Suk, J. E., Kim, D. H., Chang, J., Sung, Y. C., Choi, K. Y., and Han, K. H. (2000) Local structural elements in the mostly unstructured transcriptional activation domain of human p53. *J. Biol. Chem. 275*, 29426–29432.
35. Kussie, P. H., Gorina, S., Marechal, V., Elenbaas, B., Moreau, J., Levine, A. J., and Pavletich, N. P. (1996) Structure of the MDM2 oncoprotein bound to the p53 tumor suppressor transactivation domain. *Science 274*, 948–953.

36. Bochkareva, E., Kaustov, L., Ayed, A., Yi, G. S., Lu, Y., Pineda-Lucena, A., Liao, J. C. C., Okorokov, A. L., Milner, J., Arrowsmith, C. H., and Bochkarev, A. (2005) Single-stranded DNA mimicry in the p53 transactivation domain interaction with replication protein A. *Proc. Natl. Acad. Sci. U.S.A. 102*, 15412–15417.
37. Di Lello, P., Jenkins, L. M. M., Jones, T. N., Nguyen, B. D., Hara, T., Yamaguchi, H., Dikeakos, J. D., Appella, E., Legault, P., and Omichinski, J. G. (2006) Structure of the Tfb1/p53 complex: Insights into the interaction between the p62/Tfb1 subunit of TFIIH and the activation domain of p53. *Mol. Cell 22*, 731–740.
38. Ferreon, J. C., Lee, C. W., Arai, M., Martinez-Yamout, M. A., Dyson, H. J., and Wright, P. E. (2009) Cooperative regulation of p53 by modulation of ternary complex formation with CBP/p300 and HDM2. *Proc. Natl. Acad. Sci. U.S.A. 106*, 6591–6596.
39. Ferreon, J. C., Martinez-Yamout, M. A., Dyson, H. J., and Wright, P. E. (2009) Structural basis for subversion of cellular control mechanisms by the adenoviral E1A oncoprotein. *Proc. Natl. Acad. Sci. U.S.A. 106*, 13260–13265.
40. Feng, H., Jenkins, L. M. M., Durell, S. R., Hayashi, R., Mazur, S. J., Cherry, S., Tropea, J. E., Miller, M., Wlodawer, A., Appella, E., and Bai, Y. (2009) Structural basis for p300 Taz2-p53 TAD1 binding and modulation by phosphorylation. *Structure 17*, 202–210.
41. Dornan, D., Shimizu, H., Burch, L., Smith, A. J., and Hupp, T. R. (2003) The proline repeat domain of p53 binds directly to the transcriptional coactivator p300 and allosterically controls DNA-dependent acetylation of p53. *Mol. Cell. Biol. 23*, 8846–8861.
42. Demarest, S. J., Martinez-Yamout, M., Chung, J., Chen, H., Xu, W., Dyson, H. J., Evans, R. M., and Wright, P. E. (2002) Mutual synergistic folding in recruitment of CBP/p300 by p160 nuclear receptor coactivators. *Nature 415*, 549–553.
43. Qin, B. Y., Liu, C., Srinath, H., Lam, S. S., Correia, J. J., Derynck, R., and Lin, K. (2005) Crystal structure of IRF-3 in complex with CBP. *Structure 13*, 1269–1277.
44. Lee, C. W., Arai, M., Martinez-Yamout, M. A., Dyson, H. J., and Wright, P. E. (2009) Mapping the interactions of the p53 transactivation domain with the KIX domain of CBP. *Biochemistry 48*, 2115–2124.
45. Delaglio, F., Grzesiek, S., Vuister, G. W., Guang, Z., Pfeifer, J., and Bax, A. (1995) NMRPipe: A multidimensional spectral processing system based on UNIX pipes. *J. Biomol. NMR 6*, 277–293.
46. Johnson, B. A., and Blevins, R. A. (1994) NMRView: A computer program for the visualization and analysis of NMR data. *J. Biomol. NMR 4*, 604–613.
47. Grzesiek, S., and Bax, A. (1992) Improved 3D triple-resonance NMR techniques applied to a 31 kDa protein. *J. Magn. Reson. 96*, 432–440.
48. Wittekind, M., and Mueller, L. (1993) HNCACB, a high-sensitivity 3D NMR experiment to correlate amide-proton and nitrogen resonances with the α- and *β*-carbon resonances in proteins. *J. Magn. Reson. 101*, 201–205.
49. Bax, A., Clore, G. M., and Gronenborn, A. M. (1990) $^{1}$H-$^{1}$H correlation via isotropic mixing of $^{13}$C magnetization, a new three-dimensional approach for assigning $^{1}$H and $^{13}$C spectra of $^{13}$C-enriched proteins. *J. Magn. Reson. 88*, 425–431.
50. Grzesiek, S., Kuboniwa, H., Hinck, A. P., and Bax, A. (1995) Multiple-quantum line narrowing for measurement of Hα-H*β* J coupling in isotopically enriched proteins. *J. Am. Chem. Soc. 117*, 5312–5315.
51. Archer, S. J., Ikura, M., Torchia, D. A., and Bax, A. (1991) An alternative 3D NMR technique for correlating backbone $^{15}$N with side chain H*β* resonances in larger proteins. *J. Magn. Reson. 95*, 636–641.
52. Vuister, G. W., and Bax, A. (1993) Measurement of two- and three-bond proton to methyl-carbon J couplings in proteins uniformly enriched with $^{13}$C. *J. Magn. Reson., Ser. B 102*, 228–231.
53. Güntert, P. (2004) Automated protein structure calculation with CYANA. *Methods Mol. Biol. 278*, 353–378.
54. Herrmann, T., Güntert, P., and Wüthrich, K. (2002) Protein NMR structure determination with automated NOE assignment using the new software CANDID and the torsion angle dynamics algorithm DYANA. *J. Mol. Biol. 319*, 209–227.
55. Cornilescu, G., Delaglio, F., and Bax, A. (1999) Protein backbone angle restraints from searching a database for chemical shift and sequence homology. *J. Biomol. NMR 13*, 289–302.
56. Güntert, P., and Wüthrich, K. (1991) Improved efficiency of protein structure calculations from NMR data using the program DIANA with redundant dihedral angle constraints. *J. Biomol. NMR 1*, 447–456.
57. Case, D. A., Cheatham, T. E., III, Darden, T., Gohlke, H., Luo, R., Merz, K. M. J., Onufriev, A., Simmerling, C., Wang, B., and Woods, R. (2005) The Amber biomolecular simulation programs. *J. Comput. Chem. 26*, 1668–1688.
58. Tsui, V., and Case, D. A. (2000) Molecular simulations of nucleic acids using a generalized Born solvation model. *J. Am. Chem. Soc. 122*, 2489–2498.
59. Laskowski, R. A., Rullmann, J. A. C., MacArthur, M. W., Kaptein, R., and Thornton, J. M. (1996) AQUA and PROCHECK-NMR: Programs for checking the quality of protein structures solved by NMR. *J. Biomol. NMR 8*, 477–486.
60. Koradi, R., Billeter, M., and Wüthrich, K. (1996) MOLMOL: A program for display and analysis of macromolecular structures. *J. Mol. Graphics 14*, 51–55.
61. Wells, M., Tidow, H., Rutherford, T. J., Markwick, P., Jensen, M. R., Mylonas, E., Svergun, D. I., Blackledge, M., and Fersht, A. R. (2008) Structure of tumor suppressor p53 and its intrinsically disordered N-terminal transactivation domain. *Proc. Natl. Acad. Sci. U.S.A. 105*, 5762–5767.
62. Vise, P., Baral, B., Stancik, A., Lowry, D. F., and Daughdrill, G. W. (2007) Identifying long-range structure in the intrinsically unstructured transactivation domain of p53. *Proteins: Struct., Funct., Genet. 67*, 526–530.
63. Teufel, D. P., Freund, S. M., Bycroft, M., and Fersht, A. R. (2007) Four domains of p300 each bind tightly to a sequence spanning both transactivation subdomains of p53. *Proc. Natl. Acad. Sci. U.S.A. 104*, 7009–7014.
64. Ebert, M. O., Bae, S. H., Dyson, H. J., and Wright, P. E. (2008) NMR relaxation study of the complex formed between CBP and the activation domain of the nuclear hormone receptor coactivator ACTR. *Biochemistry 47*, 1299–1308.
65. Lees, M. J., Peet, D. J., and Whitelaw, M. L. (2003) Defining the role for XAP2 in stabilization of the dioxin receptor. *J. Biol. Chem. 278*, 35878–35888.
66. Waters, L., Yue, B., Veverka, V., Renshaw, P., Bramham, J., Matsuda, S., Frenkiel, T., Kelly, G., Muskett, F., Carr, M., and Heery, D. M. (2006) Structural diversity in p160/CREB-binding protein coactivator complexes. *J. Biol. Chem. 281*, 14787–14795.
67. Heery, D. M., Kalkhoven, E., Hoare, S., and Parker, M. G. (1997) A signature motif in transcriptional co-activators mediates binding to nuclear receptors. *Nature 387*, 733–736.
68. McInerney, E. M., Rose, D. W., Flynn, S. E., Westin, S., Mullen, T. M., Krones, A., Inostroza, J., Torchia, J., Nolte, R. T., Assa-Munt, N., Milburn, M. V., Glass, C. K., and Rosenfeld, M. G. (1998) Determinants of coactivator LXXLL motif specificity in nuclear receptor transcriptional activation. *Genes Dev. 12*, 3357–3368.
69. Voegel, J. J., Heine, M. J., Tini, M., Vivat, V., Chambon, P., and Gronemeyer, H. (1998) The coactivator TIF2 contains three nuclear receptor-binding motifs and mediates transactivation through CBP binding-dependent and -independent pathways. *EMBO J. 17*, 507–519.
70. Perissi, V., Staszewski, L. M., McInerney, E. M., Kurokawa, R., Krones, A., Rose, D. W., Lambert, M. H., Milburn, M. V., Glass, C. K., and Rosenfeld, M. G. (1999) Molecular determinants of nuclear receptor-corepressor interaction. *Genes Dev. 13*, 3198–3208.
71. Fuxreiter, M., Tompa, P., Simon, I., Uversky, V. N., Hansen, J. C., and Asturias, F. J. (2008) Malleable machines take shape in eukaryotic transcriptional regulation. *Nat. Chem. Biol. 4*, 728–737.
72. Tompa, P., and Fuxreiter, M. (2008) Fuzzy complexes: Polymorphism and structural disorder in protein-protein interactions. *Trends Biochem. Sci. 33*, 2–8.